


ARTICLE

Open Access



# SARS-CoV-2 main protease inhibitors from the stem barks of *Discoglyprena caloneura* (Pax) Prain (Euphorbiaceae) and *Pterocarpus erinaceus* Poir (Fabaceae) and their molecular docking investigation

Paul Toukam Djouonzo<sup>1\*†</sup> , Md Sofequl Islam Mukim<sup>2,3†</sup>, Pamela Nangmo Kemda<sup>1</sup>, Theodora Kopa Kowa<sup>1</sup>, Alembert Tiabou Tchinda<sup>1</sup>, Gabriel Agbor Agbor<sup>1</sup>, Cheol-Ho Pan<sup>2,3</sup> and Dae-Geun Song<sup>2,3\*</sup>

## Abstract

The main viral protease (M<sup>Pro</sup>) of SARS-CoV-2 provides an excellent target for antivirals, due to its essential and conserved function in the viral replication cycle. We reported in this study, the SARS-CoV-2 main protease inhibitory effect of twelve compounds isolated from *D. caloneura* and *P. erinaceus* together with four derivatives. Among the effectively tested samples, two derivatized compounds displayed significant improvement on the activity from the starting material, friedelin (**1**) through the acetoreduced (**2**) to the acetoxy product (**3**) with respective IC<sub>50</sub> values of 42.89, 29.69 and 19.39 µg/mL. The latter displayed the highest activity although lower as compared to that of baicalein, the positive control with IC<sub>50</sub> 0.41 µg/mL. The molecular docking study showed that an increase in the number of hydrogen bonds between compounds and active site of M<sup>Pro</sup> resulted in increased inhibition.

**Keywords** Baicalein, Derivatives, Friedelin, Molecular docking, M<sup>Pro</sup> inhibitory effect

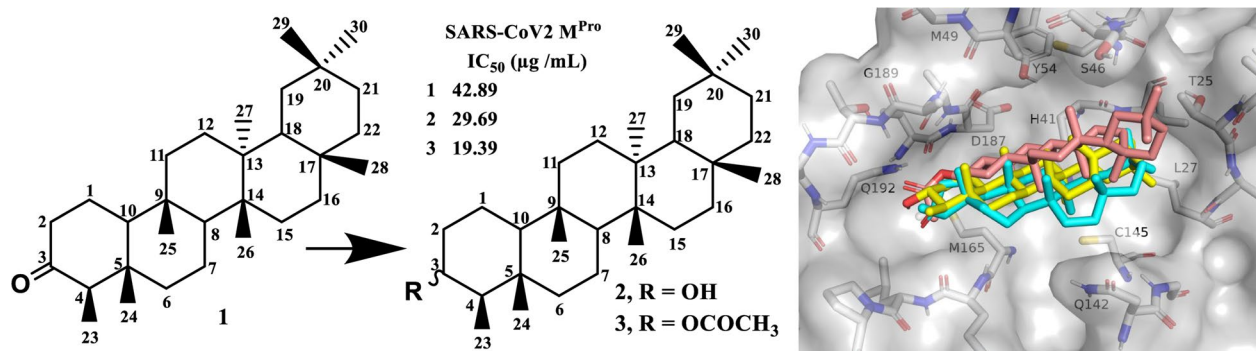
<sup>†</sup>Paul Toukam Djouonzo and Mukim Md Sofequl Islam considered as co-first authors.

\*Correspondence:

Paul Toukam Djouonzo  
tous241@yahoo.fr; paultoukam@yahoo.fr  
Dae-Geun Song  
dsong82@kist.re.kr

Full list of author information is available at the end of the article

## Graphical Abstract



## Introduction

COVID-19 is a SARS-CoV-2 viral infectious disease which emerged in early December 2019 and was proclaimed a pandemic on 12 March 2020. It caused devastating consequences worldwide, death cases were estimated in millions. This mobilised the scientific community to find effective but also quick solutions to stop the threat. In this regard, clinical trials were carried out on existing antiviral drugs some of which were homologated by the World Health Organisation (WHO) e.g., Janus Kinase (JAK) inhibitors. This is because the virus invades the immune system leading to an increase level of cytokine due to the main protease (aka M<sup>Pro</sup>, 3C-like protease, 3CL<sup>Pro</sup> or NSP5) enhancing the inflammatory process in the lung [1] through its link with Histone Deacetylase 2 [2–4]. JAK inhibitors are used to boost the immunity system and to suppress cytokine or inflammation.

In addition to anti-inflammatory drugs, several viral-protein targeting drug has been approved for treatment of COVID-19. Remdesivir was the first FDA-approved anti-viral drug for treatment of COVID-19, whose target is RNA-dependent RNA polymerase (RDRP) of SARS-CoV-2 [5]. Paxlovid has been authorized (on December 22, 2021) by the Food and Drug Administration (FDA) for COVID-19 treatment for adult and paediatric patients who are at least 12 years old and at least 40 kg body weight. It is a M<sup>Pro</sup> inhibitor who works in part by blocking a group of enzymes that are required in the metabolism of certain drugs, thereby posing a problem of

contraindication with those drugs [6]. Furthermore, Paxlovid has several side effects including allergic reactions, altered sense of taste, diarrhea, high blood pressure, muscle aches, abdominal pain, or nausea, indicating that still novel drugs must be developed.

Vaccines were equally produced which could easily be rendered ineffective due to the rapidly evolving structural proteins of the virus leading to double and triple dosage vaccine administration. As such, the search for an antiviral therapy to support the vaccine remains eminent.

The virus shows various unspecific symptoms, ranging from mild to severe and include: dry cough, fever, fatigue, sore throat and shortness of breathe [7–9]. All coronaviruses require the proteolytic activity of M<sup>Pro</sup> during virus replication, making it a high value target for the development of anti-coronavirus therapeutics [10]. Researchers also found that M<sup>Pro</sup> can indirectly affect cytokine expression; therefore, anti-inflammatory molecules as inhibitors of this enzyme may have double benefit on coronavirus patients [11]. Hence, the present study evaluated the inhibition potential of anti-inflammatory compounds previously isolated [12, 13] from *Pterocarpus erinaceus* (Poir) and *Discoglypemma caloneura* (Prain) on M<sup>Pro</sup> and evaluated the molecular docking potential of three compounds in order to speculate on the structure activity relationship observed.

*Pterocarpus erinaceus* is a small tree of 15–25 m tall, it is widely spread in the savanna zone from Senegal and Gambia to Tchad and the Central African Republic. *Discoglypemma* comprises a single species, it is a tree up to

45 m tall and occurs in rainforest and old secondary forest from east of Guinea to Uganda and south of Uganda to Democratic Republic of Congo. Their medicinal uses are multiple and include their use for the treatment of inflammation and pain [14, 15].

The investigation of their secondary metabolite led to the isolation of numerous compounds with known anti-inflammatory activities including calycosin [16], friedelin [17], aurantiamide acetate [18], acetyl aleuritolic acid [19]. To test the dual effect of the anti-inflammatory compounds, we evaluated the inhibitory effect against SARS-CoV-2 M<sup>PRO</sup>. In addition, *in silico* and *in vitro* inhibition activities of friedelin and its derivatives on human coronavirus were established by other research teams [20, 21], we found relevant to confirm their findings and speculate on the structure–activity-relationship.

## Materials and methods

### Plant material

Stem bark of *D. caloneura* and *P. erinaceus* were harvested in the month of July 2013 from Mefoup in the South Region and mount Tinguelin in the North Region of Cameroon respectively assisted by Mr Nana, botanist of the National Herbarium of Cameroon. The plants were respectively authenticated on the voucher number N°4207/SRFK and N°5205/SRFCAM at the National Herbarium Yaoundé-Cameroon.

### Extraction and isolation of compounds

The respective stem barks were chopped into small pieces, air-dried and grounded to powder. The resulting powders were successively extracted with hexane, ethyl acetate and mixture MeOH/DCM (1:1) in increasing polarity by percolation.

Compounds were isolated using chromatographic techniques such as TLC, column chromatography (normal and reversed phase) over silica gel and sephadex LH-20 with gradient and isocratic solvent systems. Compounds 1 and 4–7 were isolated from the stem bark of *P. erinaceus* [12], and 8–14 were isolated from the stem bark of *D. caloneura* [13].

### Hemisynthetic reactions

#### Reaction of reduction

Compound 1 (20 mg) was introduced into a 250 mL flask (containing some glass beads or pumice granules) with 20 mL of 95° ethanol. The compound was allowed to dissolve by heating under reflux. After complete dissolution, heat was suppressed to allow cooling at room temperature and a magnetic stirrer was placed under the flask. An amount (0.4 g) of the reducing agent, sodium tetrahydroborate (NaBH<sub>4</sub>) was added to the flask and the mixture stirred at room temperature for 10 min. Afterward,

30 mL of distilled water was added to the reaction mixture to reflux for 5 min. The mixture was cooled at room temperature for the second time and 60 mL of ice cold distilled water was added. This allowed the precipitation of the reduced compound 2 which was then recovered by filtration under vacuum while rinsing with distilled water. The filtered paper (with reduced product) was dried in a ventilated oven at 60 °C.

#### Reaction of acetylation

Compound 2 (15 mg) was allowed to react overnight with 1 mL of acetic anhydride and 0.5 mL of pyridine. After verifying the completion of reaction with TLC, an amount of distilled water (5 mL) was added to the reaction mixture and extracted with DCM using a separating funnel. The organic extract was concentrated in a rotavapor under reduced pressure. Toluene was added and evaporated three times successively to remove all traces of pyridine. Finally, the acetylated product 3 was obtained as amorphous solid or powder.

Compound 14 was treated similarly to furnish 15.

#### Reaction of methylation

A mixture of potassium carbonate (1750 mg) and dry methyl iodide (1 mL) were added to an acetone solution (15 mL) of compound 14 (20 mg). After stirring at room temperature for 10 h, the remaining acetone was evaporated in a ventilated oven at 60 °C. The residue was then dissolved in 15 mL ethyl acetate and 5 mL water was added. The organic layer was separated and dried over anhydrous magnesium sulphate. The dried organic layer was filtered and concentrated to afford the methylated product 16.

#### Cloning, protein expression and purification of M<sup>PRO</sup>

SARS-CoV-2 M<sup>PRO</sup> gene from SARS-CoV-2 isolate Wuhan-Hu-1 was ordered from Integrated DNA Technologies (<https://sg.idtdna.com/>). pET21a (+) plasmids with SARS-CoV-2 was transformed into competent cells of *E. coli* BL21(DE3). And then a fresh single colony was picked to inoculate 4 mL of liquid broth supplemented with 0.1 mg/mL Ampicillin and grown in a shaking incubator (37 °C, 180 rpm) overnight. The 4 mL inoculum / starter culture was added (1:1 ratio) to 400 mL of liquid broth with 0.1 mg/mL ampicillin and grown to an OD value of 0.4–0.5 at 600 nm, and then induced using 0.5 mM of IPTG. Afterwards, the induced cultures incubated for 3 h (37 °C, 180 rpm) and harvested (30 min, 4000 rpm, 4 °C). The harvested culture was resuspended in a lysis buffer (50 mM Tris–HCl, pH 8.0, 100 mM NaCl, 1 mM PMSF buffer) and lysed by ultrasonication (20% amplitude, 2 s on/4 s off). The cell debris was eliminated completely by centrifugation (14,000 rpm, 10 min, 4 °C).

The supernatant was incubated with Ni-NTA bead (1 h, 4 °C) on a rotator. The bead was completely washed with buffer A (50 mM Tris-HCl, pH 8.0, 300 mM NaCl, 1 mM DTT, 20 mM Imidazole); and eluted with buffer B (50 mM Tris-Cl, pH 8.0, 300 mM NaCl, 1 mM DTT, 300 mM Imidazole, 10% Glycerol). The eluted sample was concentrated via a 10,000 MWCO centrifugal concentrator spin column. Finally, desalting process was done using Fast Protein Liquid Chromatography (FPLC) to ensure high purity of the protein. The purity of the protein was further confirmed by SDS-PAGE analysis. The concentration of protein was resolved via 260 nm absorbance NanoDrop 1000 Spectrophotometer V3.8.

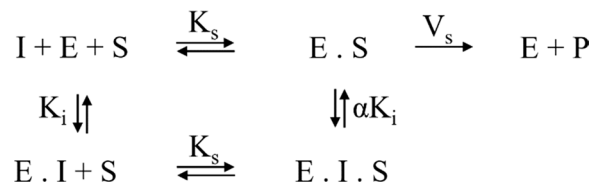
### Screening of compounds for M<sup>Pro</sup> inhibition activity

To identify inhibitors of M<sup>Pro</sup>, the FRET-based M<sup>Pro</sup> activity assay was used to screen isolated and hemi-synthetic compounds as described by Chuck and collaborators [22] with slight modification. The M<sup>Pro</sup> FRET substrate DABCYL-KTSAVLQSGFRKME- $\downarrow$ EDANS was purchased from BPS Bioscience. All compounds were stored at a stock concentration of 10 mM in DMSO. In a 96-well plate, 12.5  $\mu$ g/mL of in-house-prepared SARS-CoV-2 M<sup>Pro</sup> and 100  $\mu$ g/mL concentration of each compound was mixed in the M<sup>Pro</sup> enzyme inhibition assay in reaction buffer (20 mM Tris-Cl pH 7.4). To start the reaction, 20  $\mu$ M FRET substrate was dispensed. Following reaction initiation, fluorescence readings were taken every 1 min for a total of 30 time points using a Synergy multiplate reader (BioTek) at 360 nm excitation, and 460 nm emission. To validate our assay system, a negative control (enzyme and substrate) and a positive control (enzyme, substrate and baicalein- previously reported inhibitor) were used. For IC<sub>50</sub> value measurement, 6 different concentrations of inhibitors were used (ranging from 200  $\mu$ g/mL to 195.31 ng/mL).

### Inhibition mechanism

The study investigated the reaction velocities at different concentrations of substrate and inhibitors with a fixed concentration of enzyme. Specifically, substrate concentrations of 5, 10, 20, and 40  $\mu$ M were used, while inhibitor concentrations of 0, 40, 80, and 120  $\mu$ M were employed for Friedelin and 0, 35, 70, and 105  $\mu$ M for acetoreduced, and 0, 20, 40, and 60  $\mu$ M for acetoxy product. The collected data was globally analyzed using a generalized mixed-model of inhibition through GraphPad prism 9. This model was based on an equilibrium reaction scheme that allows for the binding of inhibitors to the free

enzyme and the enzyme-substrate complex with varying affinities. The rate equation was used to describe the different binding affinities of inhibitors, where K<sub>i</sub> represents the affinity of the inhibitor for free enzyme.



The mechanism of inhibition can be characterized by the parameter  $\alpha$ . If  $\alpha$  tends towards 1, the inhibitor can be classified as non-competitive, while if  $\alpha$  tends towards infinity, the inhibitor is considered competitive.

$$V_{obs} = \frac{[S]K_{cat}[E]_{total}}{K_m \left(1 + \frac{[I]}{K_i}\right) + [S] \left(1 + \frac{[I]}{\alpha K_i}\right)}$$

### Molecular docking simulation

Molecular docking simulation was carried out by using AutoDock VINA [23, 24]. For ligand preparation, the 3D structures of compounds were generated by using Chem3D (PerkinElmer Informatics), then pdpqt files of ligands were prepared by using prepare\_ligand4.py of AutoDock Tools. For receptor preparation, monomeric 3D structure of M<sup>Pro</sup> was extracted from a PDB structure, accession number 6M2N. Then pdpqt file was generated by using AutoDock Tools by following the author's tutorial. The center of grid box was set at -61.638, -34.761 and 23.244 in X, Y, and Z coordinates respectively. The size of the grid was set at 30 in all XYZ coordinates. Exhaustiveness was set at 16. After running the docking simulation of the ligands and the receptor, docking pose with the highest binding affinity was selected and visualized by using PyMOL (Schrodinger).

### Data analysis

IC<sub>50</sub> calculation was carried out by plotting the initial velocity versus multifarious concentrations of the compounds using Prism 9 software (Graphpad). The equation to derive IC<sub>50</sub> was four-parameter nonlinear regression equation for dose response of inhibitor.

### Results and discussion

A total of twelve compounds (1, 4–14) were previously isolated and characterised from stem barks of *P. erinaceus* [12] and *D. caloneura* [13]. Compound 1 was reduced

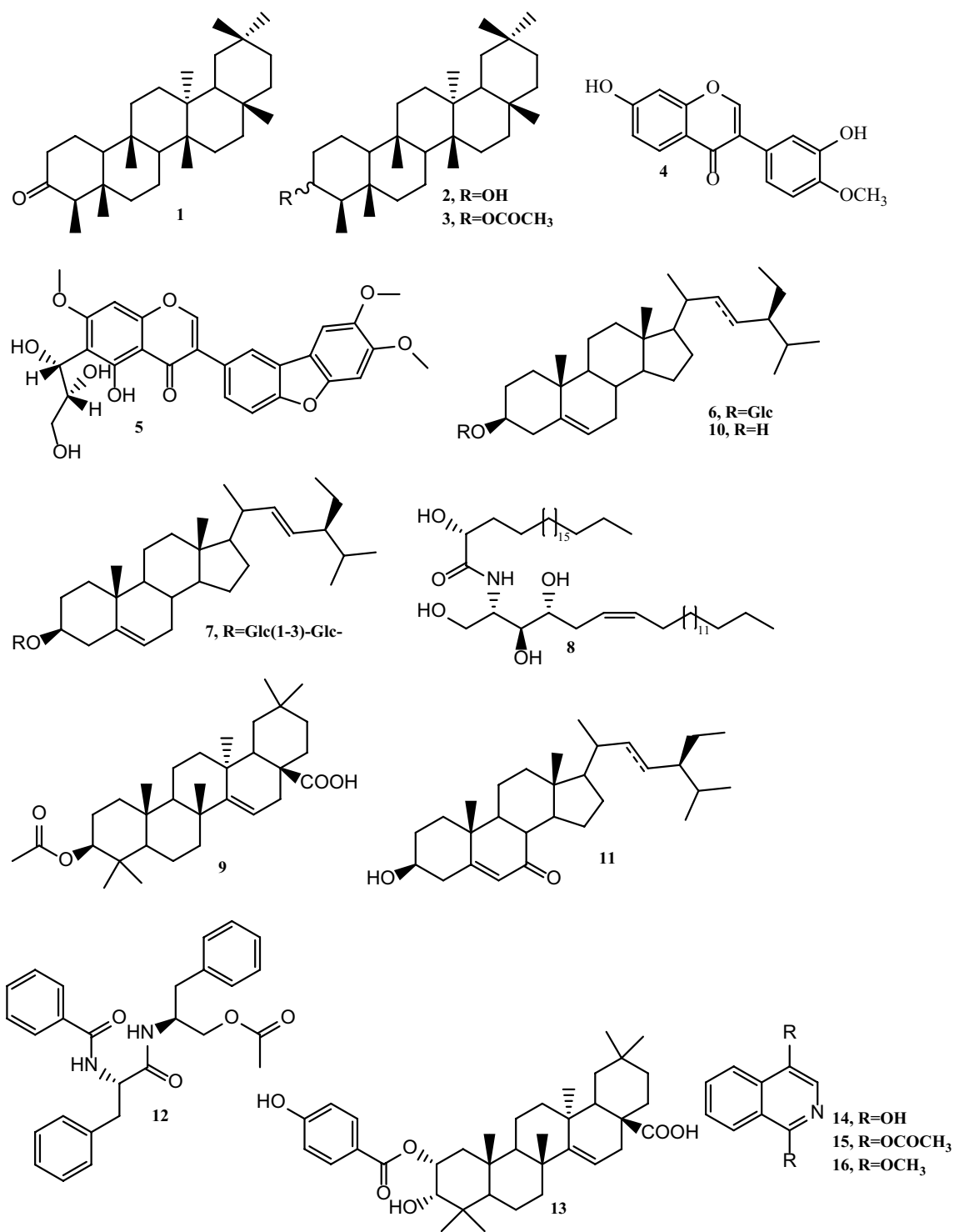


**Fig. 1** Structures of compounds (1-16)

and acetylated to furnish respectively racemic mixtures of friedelan-3-ol (**2**) and friedelan-3-acetoxy (**3**). Compound **14** was acetylated and methylated leading to compound **15** and **16** respectively. All compounds (Fig. 1) were screened for  $M^{PRO}$  inhibition potential. Inhibition kinetics and molecular docking studies were performed on compounds **1**, **2** and **3** in order to understand the significant difference in their  $M^{PRO}$  inhibition activities.

### Hemisynthetic reactions

#### Reaction of reduction of Friedelin (**1**)

The reduction of the ketone to alcohol was carried out in the presence of sodium borohydride ( $\text{NaBH}_4$ ) in ethanol under reflux. The completion of the reaction was confirmed by TLC and  $^1\text{H}$  NMR spectrum (Additional file 1: Fig. S1) which shows a broad signal at  $\delta_{\text{H}}$  3.78 corresponding to H-3 of both  $\alpha$  and  $\beta$  configuration of the racemic mixture (**2**). The reduced mixture of compounds was obtained with a yield of 95%.

#### Reaction of acetylation of the racemic mixture (**2**) and acetylation of isoquinoline-1,4-diol (**14**)

The acetylation of compound **2** was carried out overnight with acetic anhydride and pyridine. The completion of the reaction was confirmed with TLC and the presence of a sharp singlet at  $\delta_{\text{H}}$  2.2 on the  $^1\text{H}$  NMR spectrum (Additional file 1: Fig. S1). The acetylated product **3** was obtained with a yield of 80%. Compound **14** followed similar treatment as **2** and afforded compound **15** at the yield production of 82%. The  $^1\text{H}$  NMR spectrum of compound **15** (Additional file 1: Fig. S2) in addition to signals observed on the spectrum of compound **14** displayed singlet of  $\alpha$ -methyl protons at  $\delta_{\text{H}}$  2.72. Its APT spectrum (Additional file 1: Fig. S3) showed the methyl and the two carbonyl carbons respectively at  $\delta_{\text{C}}$  22.2, 165.5 and 169.8.

#### Reaction of methylation of isoquinoline-1,4-diol (**14**)

Compound **14** in the presence of methyl iodide, potassium bicarbonate and acetone afforded the methylated product **16** at the production yield of 85%. The completion of the reaction was confirmed by TLC and the presence of two methoxy protons on the  $^1\text{H}$  NMR spectrum (Additional file 1: Fig. S2) at  $\delta_{\text{H}}$  3.85 and the presence on the APT spectrum (Additional file 1: Fig. S3) of two methoxy carbons at  $\delta_{\text{C}}$  51.3 and 33.5.

### $M^{PRO}$ screening assay

Primary screening was done in fixed concentration which is 100  $\mu\text{g}/\text{ml}$ . Among them, potent compounds were further considered for secondary screening to determine  $\text{IC}_{50}$ . Compounds showing fluorescence or not dissolving neither in DMSO or pyridine were neglected for further analysis. Compounds showing fluorescence were

neglected for further analysis. They are labelled as N.A (Not applicable). Baicalein was used as a positive control and it showed  $\text{IC}_{50}$  of around 1.53  $\mu\text{M}$  which is equivalent to 0.4  $\mu\text{g}/\text{ml}$ .

Finally, we had a total of twelve compounds having effective  $\text{IC}_{50}$  values (cf Additional file 1: Table S1, Fig. 2 and Additional file 1: Fig. S4). A significant increase in activity was observed from friedelin **1** ( $\text{IC}_{50}=42.89$   $\mu\text{g}/\text{ml}$ ) to its acetoreduced derivative (**2**) ( $\text{IC}_{50}=29.69$   $\mu\text{g}/\text{ml}$ ) and acetoxy derivative **3** ( $\text{IC}_{50}=19.39$   $\mu\text{g}/\text{ml}$ ) (Fig. 2). Moderate activities were also observed with mixture of  $\beta$ -sitosterol glucoside and stigmasterol glucoside **6** ( $\text{IC}_{50}=36.45$   $\mu\text{g}/\text{ml}$ ), aurantiamide acetate **12** ( $\text{IC}_{50}=25.80$   $\mu\text{g}/\text{ml}$ ), and  $3\alpha$ -hydroxyaleuritic acid  $2\alpha$ -p-hydroxybenzoate **13** ( $\text{IC}_{50}=29.82$   $\mu\text{g}/\text{ml}$ ). Weak activities were observed with (*R*)-2-hydroxy-N-((2*S*,3*S*,4*R*,*Z*)-1,3,4-trihydroxydocos-6-en-2-yl)docosamide **8** ( $\text{IC}_{50}=49.54$   $\mu\text{g}/\text{ml}$ ), mixture of  $\beta$ -sitosterol and stigmasterol **10** ( $\text{IC}_{50}=45.17$   $\mu\text{g}/\text{ml}$ ), mixture of 7-oxo- $\beta$ -sitosterol and 7-oxo-stigmasterol **11** ( $\text{IC}_{50}=59.72$   $\mu\text{g}/\text{ml}$ ), isoquinoline-1,4-diol **14** ( $\text{IC}_{50}=41.12$   $\mu\text{g}/\text{ml}$ ), isoquinoline-1,4-diyl diacetate **15** ( $\text{IC}_{50}=63.57$   $\mu\text{g}/\text{ml}$ ), 1,4-dimethoxyisoquinoline **16** ( $\text{IC}_{50}=74.72$   $\mu\text{g}/\text{ml}$ ). Compounds with hydroxyl or sugar functions exhibited enhanced activities than their homologues lacking those functions. The enhanced activity could therefore be due to hydrogen bondings between the substrate and the target enzyme.

### Inhibition mode assays

The enzymatic kinetics approach was employed to elucidate the action mechanism of Friedelin and its two derivatives. From the mixed-model fitting result of the GraphPad Prism software, the alpha ( $\alpha$ ) values of compounds **1**, **2** and **3** were 0.55, 0.79, and 1.21, respectively (Fig. 3a, c, e). The data analysis revealed that the acetoxy product was more likely to bind to the free enzyme, as indicated by the value of  $\alpha > 1$  (Fig. 3e, f), whereas Friedelin (Fig. 3a, b), and acetoreduced product (Fig. 3c, d), were more likely to bind to the enzyme substrate complex, as indicated by the value of  $\alpha < 1$ . Despite their preferences, the  $\alpha$  values of all three were close to 1 (Fig. 3a, c, e) and double-reciprocal plots illustrated that  $K_m$  for all three compounds was dependent on the inhibitor concentration  $[I]$ , while  $V_{max}$  remained consistent (Fig. 3b, d, f). In sum, the inhibition modes of all three compounds were revealed as non-competitive.

### Molecular docking study of compound **1**, **2** and **3**

Molecular docking simulation showed that all three compounds **1**, **2**, and **3** were well fitted to the active site of  $M^{PRO}$  (Fig. 4). Of note, we used only R forms of compounds for simulation since those has less steric

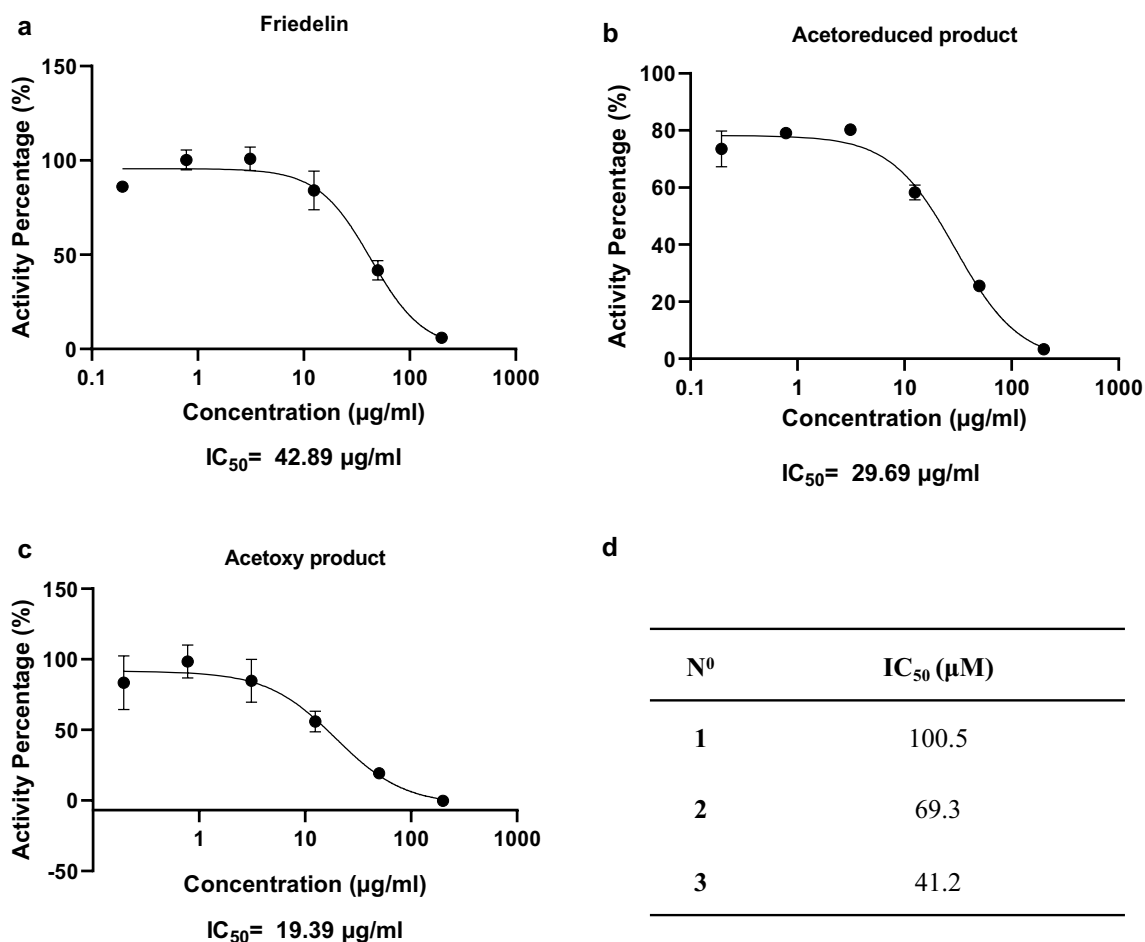


**Fig. 2** Inhibition graph and  $IC_{50}$  of Friedelin and its derivatives against SARS-CoV-2  $M^{Pro}$ . **a** Friedelin (**1**), **b** Acetoreduced friedelin (**2**), **c** Acetoxy friedelin (**3**), **d**  $IC_{50}$  in  $\mu\text{M}$

hinderance in carbon number 3. The docking score of simulation were summarized in Additional file 1: Table S2. The binding energy (affinity) of compound **3** was the lowest among compounds **1** through **3**, which is concordant to the fact that compound **3** had the lowest  $IC_{50}$  among the three. The positions of the oxygen-bound carbons number 3 were placed in S3 subsite of  $M^{Pro}$ , whereas the opposite sides (carbons number 21) were oriented toward S1 subsite of  $M^{Pro}$ . Thus, it was shown that the active site residues H41 and C145 were blocked by the interaction of inhibitors and  $M^{Pro}$ . To further analyze the structure and activity relationships, we compared the interacting residues of the carbonyl-, hydroxy-, and acetoxy- warheads of the compounds **1**, **2**, and **3**, respectively. The interactions length of less than 2.5 Å between the ligands and the enzyme residues are highlighted in yellow dashes (Fig. 4). By comparing the

warheads, compound **1** friedelin was placed closely with M165 and backbone of E166 (Fig. 4a). Unfortunately, this positioning is not favorable compared to other compounds since the partial negative charges of both carbonyl groups between friedelin and backbone of E166 may have a repulsive effect. On the other hand, hydroxy warhead of compound **2** were placed closely with Q192 (Fig. 4b) forming hydrogen bond between hydrogen atom of amide (Q192) and oxygen atom of hydroxy (Comp **2**). Finally, the acetoxy warhead of compound **3** is positioned closely with Q192 and T190 backbone (Fig. 4c). Thus, in Comp **3**, partial negative charges of oxygen atoms are available to form several hydrogen bonds with hydrogen atoms of amide residue of Q192 or amide backbone of T190. Concludingly, it is likely that increasing number of hydrogen bonds increased the affinity of friedelin

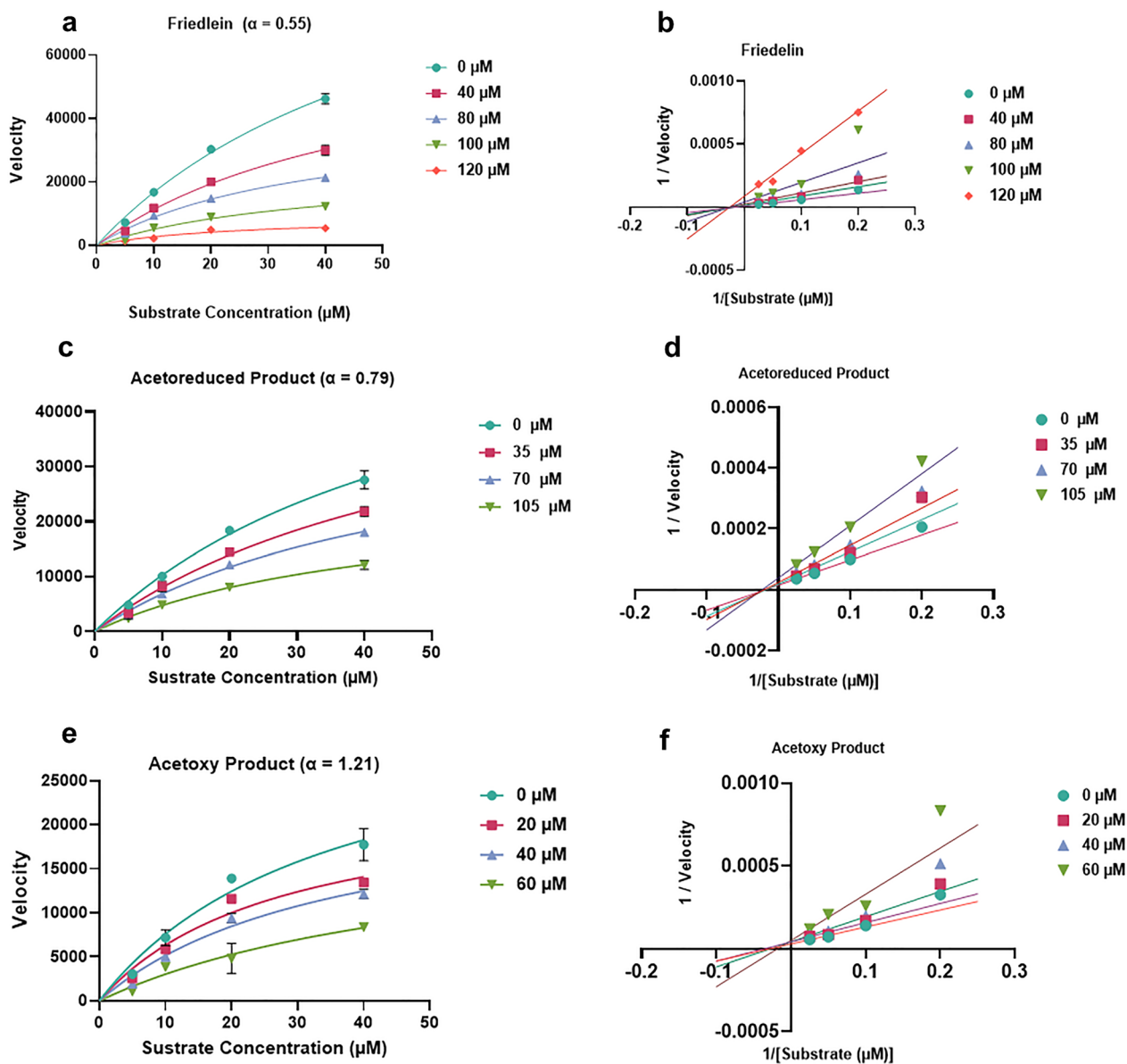


**Fig. 3** Enzyme kinetics assay. In the kinetic studies, 12.5  $\mu\text{g/ml}$   $\text{M}^{\text{P}10}$  was added to a solution containing various concentrations of substrate and protease inhibitors. **a, c, e** Lineweaver Burk Plot of the compounds (**b, d, f**)



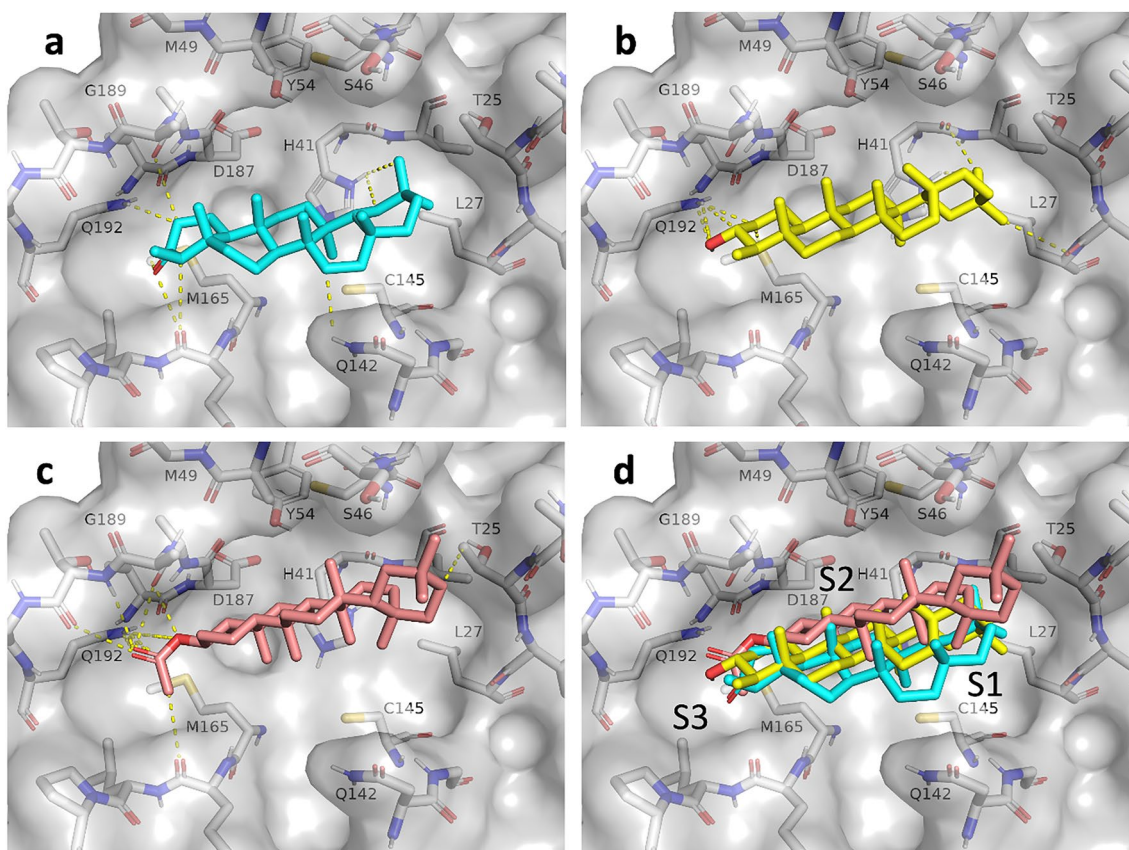


**Fig. 4** Molecular docking simulation results of Friedelin and its derivatives against SARS-CoV-2 M<sup>pro</sup>. **a** Friedelin, **b** R form of Acetoreduced friedelin, **c** R form of Acetoxy friedelin. **d** Superimpose of all three compounds. Yellow dotted line indicates close contact within 3.5 Å between compound and M<sup>pro</sup>. S1, S2, and S3 indicates the binding pocket of M<sup>pro</sup> which interacts with P1, P2, P3 residue of the peptide substrate, respectively

derivatives and eventually resulted in increased inhibitory effect against M<sup>pro</sup>.

### Supplementary Information

The online version contains supplementary material available at <https://doi.org/10.1186/s13765-023-00833-y>.

**Additional file 1. Figure S1:** Comparative <sup>1</sup>H NMR spectra of compound 1 (above), 2 (middle) and 3 (below). **Figure S2:** Comparative <sup>1</sup>H NMR spectra of compound 15 (above), 16 (middle) and 17 (below). **Figure S3:** Comparative APT spectra of compound 15 (above), 16 (middle) and 17 (below). **Table S1:** SARS-CoV-2 main protease inhibition assay results. **Table S2:** Docking score (affinity) of compounds 1, 2, 3 and baicalein by AutoDock Vina.

### Acknowledgements

Our sincere thanks to IMPM and KIST for multiple supports.

### Author contributions

PTD and MMSI: design, performed experiments, data analysis, writing original draft. PNK and TKK: design drafted manuscript. ATT and GAA: design drafted manuscript and supervise the work. CHP and DGS: acquired fundings, design drafted manuscript and supervise the work. All authors read and approved the final manuscript.

### Funding

This work was supported by Korea Institute of Science and Technology (KIST) intramural research grant and University of Science and Technology grant (2G11710 and 2021Y516) to MSI, CHP, and DGS.

### Availability of data and materials

Data will be provided upon request.

### Declarations

#### Competing interests

The authors report there are no competing interests to declare.

#### Author details

<sup>1</sup>Laboratory of Phytochemistry, Centre for Research on Medicinal Plants and Traditional Medicine, Institute of Medical Research and Medicinal Plant Studies (IMPM), P.O. Box 13033, Yaounde, Cameroon. <sup>2</sup>Natural Product Informatics Research Center, Korea Institute of Science and Technology (KIST), Gangneung Institute of Natural Products, Gangneung-si, Gangwon-do 25451, Republic of Korea. <sup>3</sup>Division of Bio-Medical Science and Technology, KIST School, Korea University of Science and Technology, Seoul 02792, Korea.

Received: 30 July 2023 Accepted: 18 October 2023

Published online: 04 November 2023

## References

- Bensussen A, Álvarez-Buylla ER, Díaz J (2021) SARS-CoV-2 Nsp5 protein causes acute lung inflammation, a dynamical mathematical model. *Front Syst Biol* 1:764155. <https://doi.org/10.3389/fsysb.2021.764155>
- Díaz J (2020) SARS-CoV-2 molecular network structure. *Front Physiol* 11:870. <https://doi.org/10.3389/fphys.2020.00870>
- Gordon DE, Jang GM, Bouhaddou M, Xu J, Obernier K, White KM et al (2020) A SARS-CoV-2 protein interaction map reveals targets for drug repurposing. *Nature* 583(7816):459–468. <https://doi.org/10.1038/s41586-020-2286-9>
- Hekman RM, Hume AJ, Goel RK, Abo KM, Huang J, Blum BC et al (2020) Actionable cytopathogenic host responses of human alveolar type 2 cells to SARS-CoV-2. *Mol Cell* 80(6):1104–1122. <https://doi.org/10.1016/j.molcel.2020.11.028>
- Beigel JH, Tomashek KM, Dodd LE, Mehta AK, Zingman BS, Kalil AC, Hohmann E, Chu HY, Luetkemeyer A, Kline S et al (2020) Remdesivir for the treatment of covid-19 - final report. *N Engl J Med* 383:1813–1826. <https://doi.org/10.1056/nejmoa2007764>
- FDA (2022) The FDA news release. <https://www.fda.gov/news-events/press-announcements/coronavirus-covid-19-update-fda-authorizes-first-oral-antiviral-treatment-covid-19>. Accessed 17 Feb 2023
- Huang C, Wang Y, Li X, Ren L, Zhao J, Hu Y, Zhang L, Fan G, Xu J, Gu X, Cheng Z, Yu T, Xia J, Wei Y, Wu W, Xie X, Yin W, Li H, Liu M, Xiao Y, Gao H, Guo L, Xie J, Wang G, Jiang R, Gao Z, Jin Q, Wang J, Cao B (2020) Clinical features of patients infected with 2019 novel coronavirus in Wuhan, China. *Lancet* 395(10223):497–506. [https://doi.org/10.1016/s0140-6736\(20\)30183-5](https://doi.org/10.1016/s0140-6736(20)30183-5)
- Yuki K, Fujiogi M, Koutsogiannaki S (2020) COVID-19 pathophysiology: a review. *Clin Immunol* 215:108427. <https://doi.org/10.1016/j.clim.2020.108427>
- Attaway AH, Scheraga RG, Bhimraj A, Biehl M, Hatipoğlu U (2021) Severe covid-19 pneumonia: pathogenesis and clinical management. *BMJ*. <https://doi.org/10.1136/bmj.n436>
- Clifford F (2020) Screening potential anti-virals for the main protease of the Coronaviridae family including SARS-CoV-2, SARS-CoV, MERS. [Research Report] Eigenenergy South Australia. hal-02897882ff. <https://hal.science/hal-02897882/document>
- Zhu J, Zhang H, Lin Q, Lyu J, Lu L, Chen H, Zhang X, Zhang Y, Chen K (2022) Progress on SARS-CoV-2 3CLpro inhibitors: inspiration from SARS-CoV 3CLpro peptidomimetics and small-molecule anti-inflammatory compounds. *Drug Des Dev Ther* 16:1067–1082. <https://doi.org/10.2147/dddt.s359009>
- Toukam DP, Tagatsing FM, Tchokouaha YLR, Baishya G, Barua NC, Tchinda TA, Mbafor TJ (2018) Novel saponin and benzofuran isoflavonoid with in vitro anti-inflammatory and free radical scavenging activities from the stem bark of *Pterocarpus erinaceus* (Poir). *Phytochem Lett* 28:69–75. <https://doi.org/10.1016/j.phytol.2018.09.006>
- Toukam DP, Kom WC, Tchamgoué DA, Doupno KEA, Younoussa L, Tchokouaha YLR, Kopa KT, Tchinda TA, Frédéric M, Mbafor TJ, Atchadé ADT (2021) A new isoquinoline and ceramide from the stem barks of *Discoglyprena caloneura* (Pax) Prain (Euphorbiaceae) with antiproteinase and cytotoxic activities. *Nat Prod Res* 36(1):1–9. <https://doi.org/10.1080/14786419.2021.1890073>
- Duval CS (2008) *Pterocarpus erinaceus* Poir. In: Louppe D, Oteng-Amoako AA, Brink M (eds) PROTA (Plant Resources of Tropical Africa/Ressources végétales de l'Afrique tropicale), Wageningen, Netherlands. [https://uses.plantnet-project.org/en/Pterocarpus\\_erinaceus\\_\(PROTA\)](https://uses.plantnet-project.org/en/Pterocarpus_erinaceus_(PROTA)). Accessed 5 Oct 2023
- Schmelzer GH (2008) *Discoglyprena caloneura* (Pax) Prain. In: Schmelzer GH & Gurib Fakim A (Editors). PROTA (Plant Resources of Tropical Africa/Ressources végétales de l'Afrique tropicale), Wageningen, Netherlands. [https://uses.plantnet-project.org/en/Discoglyprena\\_caloneura\\_\(PROTA\)](https://uses.plantnet-project.org/en/Discoglyprena_caloneura_(PROTA)). Accessed 5 Oct 2023
- Mao D, Huijuan C, Jiaying L, Jiawen S, Long X, Xiaofang L (2020) Calycosin: a review of its pharmacological effects and application prospects, expert review of anti-infective therapy. *Nat Prod Res* 19(7):911–925. <https://doi.org/10.1080/14787210.2021.1863145>
- Antonisamy P, Duraipandiyar V, Ignacimuthu S (2011) Anti-inflammatory, analgesic and antipyretic effects of Friedelin isolated from *Azima tetraacantha* Lam. in mouse and rat models. *J Pharm Pharmacol* 63(8):1070–1077. <https://doi.org/10.1111/j.2042-7158.2011.01300.x>
- Fang Z, Fang J, Gao C, Wu Y, Yu W (2022) Aurantiamide acetate ameliorates lung inflammation in lipopolysaccharide-induced acute lung injury in mice. *Biomed Res Int* 2022:1–8. <https://doi.org/10.1155/2022/3510423>
- Bezerra AJN, Silva FCO, da Silva AW, Ferreira MKA, Marinho EM, Marinho MM et al (2021) Antinociceptive effect of triterpene acetyl aleuritic acid isolated from *Croton zehntneri* in adult zebrafish (*Danio rerio*). *Biochem Biophys Res Commun* 534:478–484. <https://doi.org/10.1016/j.bbrc.2020.11.056>
- Kar P, Sharma NR, Singh B, Sen A, Roy A (2021) Natural compounds from *Clerodendrum* spp. as possible therapeutic candidates against SARS-CoV-2: an in silico investigation. *J Biomol Struct Dyn* 39(13):4774–4785. <https://doi.org/10.1080/07391102.2020.1780947>
- Chang FR, Yen CT, Ei-Shazly M, Lin WH, Yen MH, Lin KH, Wu YC (2012) Anti-human coronavirus (ant-HCoV) triterpenoids from the leaves of *Euphorbia neriifolia*. *Nat Prod Commun* 7(11):1415–1417. <https://doi.org/10.1177/1934578x1200701103>
- Chuck CP, Chow HF, Wan DCC, Wong KB (2011) Profiling of substrate specificities of 3C-like proteases from group 1, 2a, 2b, and 3 coronaviruses. *PLoS ONE* 6(11):e27228. <https://doi.org/10.1371/journal.pone.0027228>
- Trott O, Olson AJ (2010) AutoDock Vina: improving the speed and accuracy of docking with a new scoring function, efficient optimization and multithreading. *J Comput Chem* 31(2):455–461. <https://doi.org/10.1002/jcc.21334>
- Eberhardt J, Santos-Martins D, Tillack AF, Forli S (2021) AutoDock Vina 1.2.0: new docking methods, expanded force field, and python bindings. *J Chem Inf Model* 61(8):3891–3898. <https://doi.org/10.1021/acs.jcim.1c00203>

## Publisher's Note

Springer Nature remains neutral with regard to jurisdictional claims in published maps and institutional affiliations.

Submit your manuscript to a SpringerOpen® journal and benefit from:

- Convenient online submission
- Rigorous peer review
- Open access: articles freely available online
- High visibility within the field
- Retaining the copyright to your article

Submit your next manuscript at ► [springeropen.com](https://www.springeropen.com)